Adsorptive Removal of Heavy Metal from Acidic Wastewater with Biochar Produced from Anaerobically Digested Residues: Kinetics and Surface Complexation Modeling

Youchi Zhang and Wensui Luo *

In this study, the adsorptive characteristics of biochar generated from anaerobically digested garden wastes (AD-char) were investigated. Metal adsorption onto AD-chars reached equilibrium in 48 h; the adsorption capacity of Cu^{2+} by AD-char was 182 μmol g^{-1}, which was higher than that of Zn^{2+} (35.3 μmol g^{-1}) and Mn^{2+} (60.7 μmol g^{-1}). The metal adsorption was well described by the pseudo second-order kinetic and Langmuir isotherm models. pK^{int}_{a1}, pK^{int}_{a2}, and pk_{Cu} for AD-char, which described surface protonation reactions and complexation with Cu^{2+}, were 5.75, -10.20, and -4.70, respectively, as optimized by the surface complexation model. Cu^{2+} adsorption onto AD-char increased with increasing pH to < 8.6, which suggests that the presence of surface alkaline functional groups can be attributed to the metal adsorption capacity of biochar. This study concluded that converting anaerobically digested food and garden wastes into biochar could be an efficient method of treating municipal solid waste and producing metal adsorbents for environmental remediation.

Keywords: Biochar; Metal adsorbent; Anaerobic digestion residue; Copper removal; Surface complexation model

*Contact information: Institute of Urban Environment, Chinese Academy of Sciences, No. 1799, Jimei Road, Xiamen 361021, P. R. China; *Corresponding author: wsluo@iue.ac.cn*

INTRODUCTION

Anaerobic digestion (AD) is an efficient municipal and agricultural organic waste recycling technique (Zhang *et al*. 2007; Rapport *et al*. 2012). However, AD residue treatment is a challenging task, as a high volume of substrates remains in the reactor at the end of digestion (Yuan *et al.* 2011). One of the promising approaches to AD residue treatment is to convert carbon-rich AD residue to biochar using pyrogenic processes under oxygen-limited environments (Lehmann *et al*. 2011). Biochar production and utilization has attracted attention because biochar can improve soil fertility and serve as recalcitrant carbon stocks to prevent global warming (Beesley *et al*. 2011). If AD residue can be used as feedstock for biochar production, it would provide additional value for waste treatment (Inyang *et al*. 2012).

Biochar can be an efficient sorbent for removing heavy metals from wastewater (Cao *et al*. 2009; Dong *et al*. 2011). However, the adsorption capacity of biochars varies with physicochemical properties such as pH, surface area, and functional groups that depend on raw materials and production procedures (Zhao *et al*. 2013; Melo *et al*. 2013). For instance, variation in surface adsorptive site density results in different metal ion adsorptions by biochars (Xue *et al*. 2012), while the diversity of surface functional groups leads to different metal adsorption mechanisms (Qiu *et al*. 2008). Xu *et al*. (2012) found that dairy manure-derived biochars mainly retained metal ions through surface precipitation as metal carbonates and phosphates. Jiang *et al*. (2012) illustrated Pb^{2+} adsorption with rice straw-derived biochar *via* surface complexation with delocalized π electrons. Garden waste, such as wood bark, has a unique lignocellulose structure, which leads to specific adsorptive sites with the produced biochars (Sud *et al*. 2008; Mukome *et al*. 2013). Food waste contained a lot of organic constituents (Arvanitoyannis and Varzakas 2008), so the mixing of food waste and garden green waste as biochar feedstock may increase the adsorptive site of biochar. In addition, AD treatment can change the characteristics of raw materials by enhancing the densities of exchangeable cation ions (Hanay *et al*. 2008; Yao *et al*. 2011) or utilizing labile pore in-filling organic matter (Inyang *et al.* 2010), which leaves the refractory pore framework intact. Thus, biogas residue-derived biochar may possess different metal adsorption capacities from those made from raw materials.

In this study, the AD residue of garden waste was used as a feedstock to produce biochar, and the kinetic and adsorptive characteristics with respect to the metal ions Cu^{2+}, Zn^{2+}, and Mn^{2+} were investigated in comparison with biochar made directly from garden green waste (*Eucalyptus* leaves). Kinetic and isotherm models such as the Lagergen pseudo first-order kinetic model, Ho pseudo second-order kinetic model, Freundlich isotherm, and Langmuir isotherm were used to fit the metal adsorption results, providing information about adsorption affinity and saturation capacity (Xu *et al*. 2012). The surface complexation model (SCM), which is a useful tool for simulating the chemical properties of complex surfaces of adsorbents and metal partitioning among aqueous/solid phases (Robertson and Leckie 1997), was used to calculate metal ion speciation in solution/biochar systems. This study aimed to provide more knowledge about the potential of the utilization of AD residue to produce effective metal sorbents through the biochar process in particular the metal adsorption mechanism by such biochar, which would expand the re-use approaches of municipal solid waste (MSW).

MATERIALS AND METHODS

Biochar Preparation

Anaerobic digestion residues were obtained from a midscale reactor using food waste and garden waste as substrates to produce the AD-char, in which the anaerobic digestion was conducted in mesophilic temperature 37 °C with 5% sludge from a waste treatment plant as the inoculum. *Eucalyptus* leaves were collected from a garden in Xiamen, southern China to produce the E-char. Before carbonization, the feedstock was ground and sieved through a 50-mm mesh screen. A rotary pyrolyzer, which consists of a gas combustion system, automatic temperature control system, mechanical mixing system, and rotary furnace body with an effective volume of 75 L, was used. To produce biochars under limited O_2 conditions, the furnace body was almost completed closed with several layers asbestos cloth to cover the gaps, leaving a small tube for gas emission. The feedstock was placed in the rotary carbonization chamber and dried at 200 °C for 1 h at the initial stage (drying at 200 °C is considered torrefaction, during which hemicellulose undergoes limited devolatilization and carbonization (Cao and Harris 2010). The temperature was further raised to 400 °C at a rate of 5 °C min^{-1} and maintained for 0.5 h

(Sun *et al*. 2013). After cooling to room temperature, the biochars were collected from the pyrolyzer, gently ground, and then sieved through a 20-mesh screen (< 0.85 mm).

Characterization

The pH of the biochar was determined at a 1:5 solids-to-deionized water ratio. Structural characteristics were measured by nitrogen adsorption isotherms at 77 K using a surface area and porosimetry analyzer (ASAP2020 M + C; Micromeritics, USA). Elemental (C, H, and O) analyses were conducted using a CHNS/O Analyzer (Vario MAX; Elementar, Germany). Other elements (Ca, Mg, K, Na, etc.) were determined using HNO_3-$HClO_4$ digestion – ICP-OES analysis (Optima 7000DV; Perkin Elmer, USA). Fourier transform infrared (FTIR) analysis of the biochar was carried out using a FTIR spectrometer (Nicolet iS10; Thermo Fisher Scientific, USA), while the Boehm titration method was used to analyze the amounts of surface functional groups (carboxyl, lactonic, phenolic, and base groups) (Qiu *et al*. 2008). Scanning electron microscopy (SEM) was used to examine the surface morphology of biochars. The proton neutralization capacity of biochar was measured through a pH titration method following a protocol of Rangel-Mendez and Streat (2002) with modifications. In brief, 5 mL of 0.01 M $NaNO_3$ solutions with different initial pH values (adjusted with a HCl or NaOH solution) were added to test tubes together with 0.05 g biochar. After shaking at a constant speed of 200 rpm for 72 h, the equilibrium pH values were measured.

Adsorption Kinetics Experiments

The kinetics experiments were performed in 100-mL centrifuge tubes at 25 °C. One-half gram of biochar was mixed with 50 mL of wastewater with an electrolyte background of 0.01 M $NaNO_3$. The waste water was synthesized in the lab, in which the metal ions Cu^{2+}, Zn^{2+}, and Mn^{2+} were chosen since they were three major contaminants of an acidic mining drainage from a nearby metal mine located in Da`tian, south China (Xu *et al.* 2003). The initial concentration of Cu^{2+}, Zn^{2+}, or Mn^{2+} ion in wastewater was 25 mg L^{-1}, while the initial pH was 4.6±0.2. Then, the mixture was shaken at a constant speed of 200 rpm, and the samples were collected at different time intervals. Afterwards, the samples were filtered through a 0.45-μm cellulose nitrate membrane and immediately acidified to pH < 2 with an HNO_3 solution for analysis. Cu^{2+}, Zn^{2+}, and Mn^{2+} concentrations in the filtrate were measured by ICP-OES. Triplicates were prepared for each treatment. In addition, less than 10 μg/L of Cu^{2+}, Zn^{2+}, or Mn^{2+} ion would be leached from the biochars in the preliminary blank experiment.

Adsorption Isotherm Experiments

The adsorption isotherms were determined in a background electrolyte of 0.01 M $NaNO_3$ at 25 °C. A 5-mL aliquot of 10 g/L biochar was transferred to a 15-mL centrifuge tube. Cu^{2+}, Zn^{2+}, and Mn^{2+} concentration ratios in wastewater were similar to those used in adsorption kinetics experiments with an initial pH of 4.6±0.2. After shaking at 200 rpm for 48 h, the samples were collected, and the Cu^{2+}, Zn^{2+}, and Mn^{2+} concentrations were measured. Triplicates were prepared for each treatment.

Influence of Initial Solution pH on Metal Adsorption onto Biochars

In a 15-mL centrifuge tube, a 5-mL aliquot of 10 g L^{-1} biochar was shaken at 200 rpm for 48 h. Afterward, the samples were collected, in which the metal concentrations and pH values were measured. The initial concentration of metal ions in wastewater was the same as that used in adsorption kinetics experiments. Three levels of initial solution pH used in the experiment were pH 3, pH 4.6, and pH 6. Triplicates were prepared for each treatment.

Applied Adsorption Models

Adsorption kinetics models

The kinetics experimental results were fitted by Lagergen pseudo first-order [Eq. (1)] and Ho pseudo second-order kinetic models [Eq. (2)] using OriginPro 8.0 (OriginLab Corporation, MA, USA).

The Lagergen pseudo first-order kinetics model (Mohan *et al*. 2012), which assumes that physical adsorption occurred and the solute uptake rate with time is directly proportional to the ratio of the solute concentration and the amount of solids, can be expressed as

$$q_t = q_e(1 - e^{-k_1 t}) \quad (1)$$

where k_1 is the rate constant (h^{-1}), q_e is the amount adsorbed at equilibrium (mmol g^{-1}), and q_t is the amount adsorbed at time t (mmol g^{-1}).

The Ho pseudo second-order kinetics model (Ho 2006), which assumes that chemisorption occurred, in which inner-sphere complexation and precipitation involved metal ion sorption, whereas the role of electrostatic ion exchange could be negligible, can be expressed as

$$\frac{t}{q_t} = \frac{1}{k_2 q_e^2} + \frac{t}{q_e} \quad (2)$$

where k_2 is the rate constant (g $mmol^{-1}$ min^{-1}), q_e is the amount adsorbed at equilibrium (mmol g^{-1}), and q_t is the amount adsorbed at time t (mmol g^{-1}).

Adsorption isotherm models

The adsorption isotherm data were analyzed using Freundlich [Eq. (3)] and Langmuir [Eq. (4)] isotherm models and calculated using OriginPro 8.0 (OriginLab Corporation, MA, USA).

The Freundlich isotherm model (Mohan *et al*. 2012), which assumes heterogeneous adsorptive energies on the adsorbent surface, can be expressed as

$$q_e = k_F C_e^{1/n} \quad (3)$$

where q_e is the amount adsorbed per unit weight of adsorbent (mmol g^{-1}), C_e is the equilibrium concentration in the solution (mmol L^{-1}), the constant k_F indicates the adsorbent's relative adsorption capacity (mmol g^{-1}), and $1/n$ is a constant that represents adsorption intensity.

The Langmuir isotherm model (Mohan *et al*. 2012), which assumes homogeneous monolayer surface sorption, can be expressed as

$$q_e = \frac{Q^0 b C_e}{1 + b C_e} \quad (4)$$

where q_e is the amount adsorbed per unit weight of adsorbent (mmol g^{-1}), C_e is the equilibrium concentration in the solution (mmol L^{-1}), Q^0 is the monolayer adsorption capacity (mmol g^{-1}), and the constant b is related to the net enthalpy of adsorption.

Surface complexing model

The SCM is based on the theory that surface functional groups can be divided into three species (negative XO^-, neutral XOH, positive XOH_2^+) according to protonation reactions [Eqs. (a) and (b)], while metal adsorption primarily occurs *via* complexation with surface functional groups [Eq. (c)] (Al-Hamdan and Reddy 2005). Based on the specific surface parameters pK^{int}_{a1}, pK^{int}_{a2}, and pK_M, as well as the metal hydrolysis constants pK_{MOH+} and $pK_{M(OH)2}$, metal speciation in the aqueous/soil phase was simulated by FITEQL 4.0, developed by Herbelin and Westall (1999). Instead of experimental kinetics or isotherm models, SCM can simulate the change in surface functional groups and the speciation of metal elements with changing solution conditions, such as pH and electrolyte concentrations (Guo *et al*. 2008), thereby clarifying the metal adsorption mechanism.

$$XOH_2^+ = XOH + H^+ \tag{a}$$

$$pK_{a1}^{int} = -\mathrm{Log}\frac{\{XOH\}\{H^+\}}{\{XOH_2^+\}}$$

$$XO^- + H^+ = XOH \tag{b}$$

$$pK_{a2}^{int} = -\mathrm{Log}\frac{\{XOH\}}{\{XO^-\}\{H^+\}}$$

$$XOH + M^{2+} = XOM^+ + H^+ \tag{c}$$

$$pK_M = -\mathrm{Log}\frac{\{XOM^+\}\{H^+\}}{\{XOH\}\{M^{2+}\}}$$

$$M^{2+} + H_2O = MOH^+ + H^+ \tag{d}$$

$$pK_{M\,OH^+} = -\mathrm{Log}\frac{\{MOH^+\}\{H^+\}}{\{M^{2+}\}\{H_2O\}}$$

$$M^{2+} + 2H_2O = M(OH)_2 + 2H^+ \tag{e}$$

$$pK_{M\,(OH)_2} = -\mathrm{Log}\frac{\{M(OH)_2\}\{H^+\}\{H^+\}}{\{M^{2+}\}\{H_2O\}\{H_2O\}}$$

RESULTS AND DISCUSSION

Characteristics of Biochars

As shown in Table 1, carbon was the major element constituent of AD-char or E-char, which indicates that biochars exhibit significant carbonaceous properties. As shown by SEM (Fig. 1), both the biochars had well-developed pore structure. The Brunauer–Emmett–Teller surface areas of AD-char and E-char were 7.60 and 10.35 $m^2\ g^{-1}$, respectively. The porosity of AD-char was twice that of E-char, while its average pore diameter was 6.70 nm, which is larger than that of E-char (2.29 nm).

According to FITR analysis (Fig. 2), the infrared spectra of AD-char and E-char showed similar bands at 669, 1120, 1380, 1510, 1560, 1650, and 2360 cm^{-1}. As reported in previous research (Gupta *et al*. 2012; Sun *et al*. 2013), the bands at 669 and 1380 cm^{-1} were assigned to the C-H bond out-of-plane bending of alkenes and in-plane bending vibration of alkanes. The band at 1120 cm^{-1} was assigned to C=O stretching and bending of ketones. The band at 1510 cm^{-1} was assigned to the vibration ($\nu_{C=C}$) of the benzene carbon skeleton. The band at 1560 cm^{-1} was attributed to the C=O stretching of carboxyl anions. The band at 1650 cm^{-1} was assigned to stretching (ν) (C=O) vibration of carbonyl groups. The band at 2360 cm^{-1} was attributed to the C–O vibrations in the carbon dioxide molecule. In addition, as suggested by the Boehm titration results (Table 1), the AD-char content of the total surface functional group was 5.35±0.21 mmol g^{-1}, while the E-char content was 3.05±0.14 mmol g^{-1}. AD-char contained more carboxyl, phenolic, and base groups, but had fewer lactonic groups. The differences in the composition of surface functional groups were attributed to the variety of feedstock, which could further influence the metal retention capacity of biochars.

Table 1. Characteristics of Biochars

Item		**E-char**	**AD-char**
pH		7.47±0.01	8.83±0.06
Element composition			
C	%	75.5±2.1	60.3±0.5
H		3.6±0.1	4.0±0.05
O		16.4±1.5	22.3±1.3
N		1.1±0.05	1.92±0.03
Al	mg g^{-1}	0.085±0.004	0.96±0.08
Fe		0.003±0.001	3.22±1.66
Na		1.04±0.23	14.71±6.56
K		1.74±0.42	3.42±1.28
Ca		5.55±0.44	48.2±27.0
Mg		0.76±0.19	1.79±0.82
Structure characteristics			
BET surface area	m^2 g^{-1}	10.35	7.6
Porosity	cm^3 g^{-1}	0.006	0.013
Average pore size	Nm	2.29	6.7
Surface acidity/basicity			
Carboxyl group	mmol g^{-1}	0.40±0.00	0.95±0.07
Lactonic group		0.93±0.04	0.18±0.03
Phenolic group		0.02±0.03	0.78±0.10
Total acid group		1.35±0.07	1.90±0.14
Base group		0.35±0.07	1.55±0.07
Total surface functional group		3.05±0.14	5.35±0.21

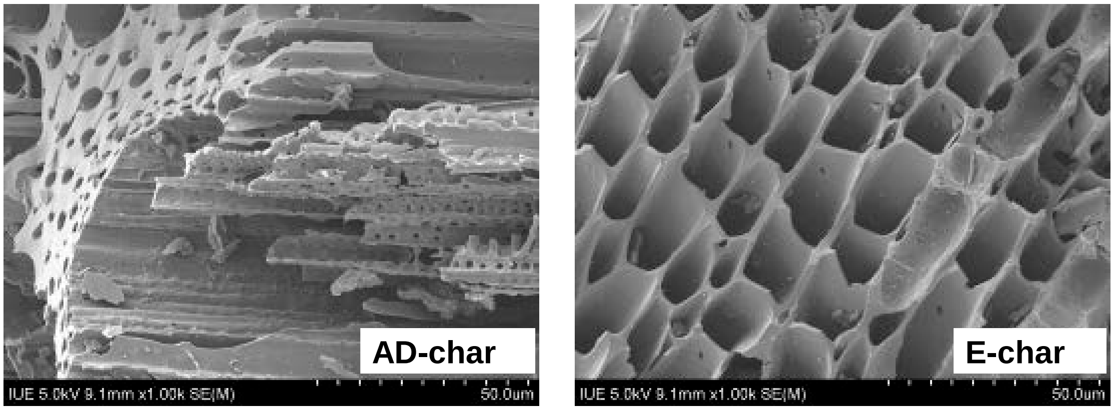

Fig. 1. SEM images of biochars

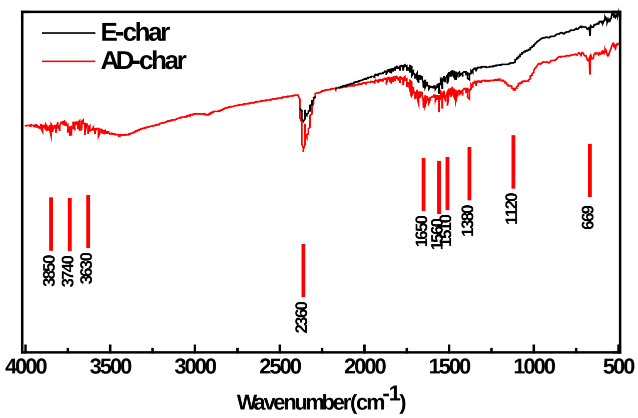

Fig. 2. FTIR spectra of biochars

Adsorption Kinetics of Metals onto Biochars

The kinetics of biochars in metal ion removal are shown in Fig. 3. Cu^{2+}, Zn^{2+}, and Mn^{2+} adsorption onto either AD-char or E-char reached equilibrium in 48 h, while metal ion adsorption onto AD-char was higher than on E-char. The adsorption kinetics of metal ions by biochars was better described by the pseudo second-order model (R^2=0.86~0.99) than by the pseudo first-order model (R^2=0.50–0.92) (Table 2). The pseudo second-order model assumed that chemisorption was the rate-limiting step of adsorption (Ho 2006). Thus, this result suggests that the adsorption of Cu^{2+}, Zn^{2+}, and Mn^{2+} ions onto biochar was primarily controlled by the chemical reaction, depending on the distribution of surface functional groups on biochars (Qiu *et al*. 2008). For instance, the carboxyl group on the biochar surface, as indicated by the FITR results, played a role in metal ion bonding onto the adsorbent (Uchimiya *et al.* 2010). Thus, the higher carboxyl group content in AD-char, which was more than twice that in E-char (Table 1), might partially explain the higher metal ion adsorption onto AD-char.

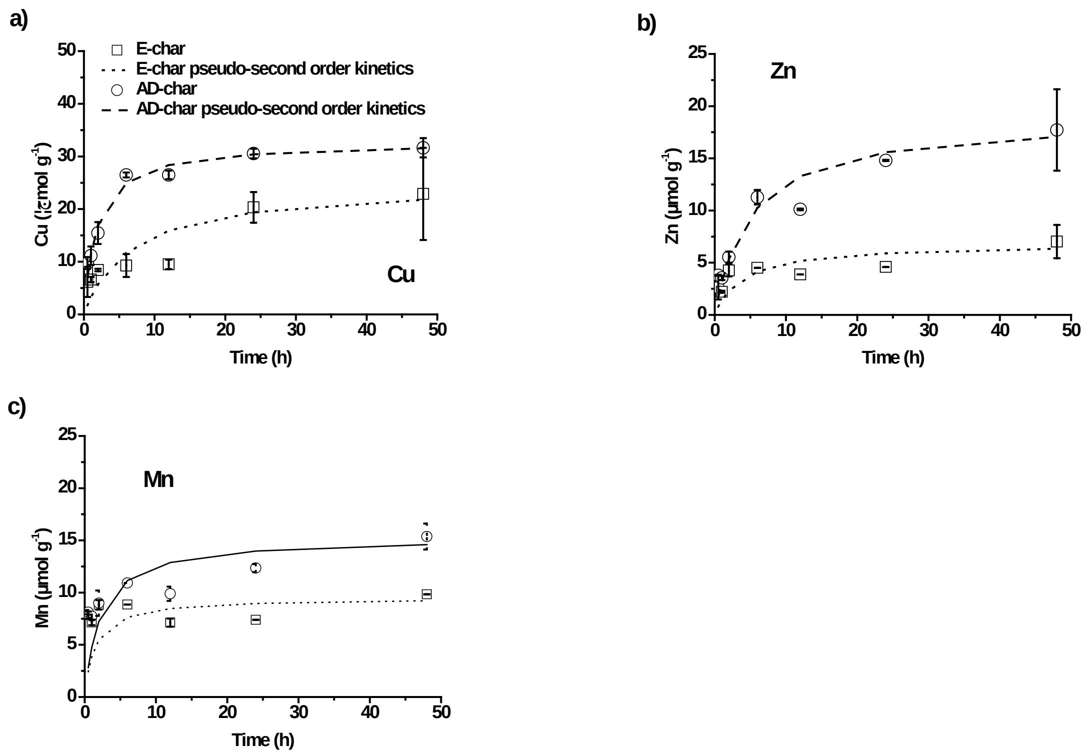

Fig. 3. Adsorption kinetics of metals onto biochars

Table 2. Fitted Kinetics Models for Metal Adsorption on Biochars

	Biochar	Pseudo first-order kinetics model			Pseudo second-order kinetics model		
		k_1 (hr^{-1})	q_e (μmol g^{-1})	R^2	k_2 (g $μmol^{-1}$ hr^{-1})	q_e (μmol g^{-1})	R^2
Cu	E-char	0.08	22.72	0.57	0.006	24.82	0.86
	AD-char	0.45	29.34	0.92	0.016	32.79	0.99
Zn	E-char	2.87	8.00	0.87	0.038	6.85	0.92
	AD-char	0.19	15.33	0.82	0.011	18.85	0.97
Mn	E-char	3.85	9.18	0.50	0.072	9.50	0.97
	AD-char	0.72	12.93	0.56	0.030	15.23	0.97

Adsorption Isotherms of Metals onto Biochars

The adsorption isotherms of metal ions onto biochars are shown in Fig. 4. Cu^{2+} adsorption increased with increasing aqueous concentration. At equilibrium, Cu^{2+} adsorption onto AD-char was about 182 μmol g^{-1} (11.6 mg g^{-1}), while adsorption onto E-char was about 160 μmol g^{-1} (10.2 mg g^{-1}). $Zn^{2+}$and Mn^{2+} adsorptions at equilibrium were 35.3 and 60.7 μmol g^{-1}, respectively, for AD-char, and 30.6 and 61.6 μmol g^{-1}, respectively, for E-char, far lower than for Cu^{2+} adsorption. According to the differences in ion radius and hydrolysis properties of metals (Table 3), Cu^{2+} had the highest adsorption affinity among the three metals partially due to its lowest value of hydrated ion radius, which may lead to the predominant Cu^{2+} adsorption.

Compared with previous research (Table 4), the adsorption capacity of Cu^{2+} ions onto AD-char was 2.5 to 5.5 times that of raw MSW, including food waste and cellulose pulp waste (Ulmanu *et al*. 2003; Zheng *et al*. 2008). In addition, the adsorption capacity of Cu^{2+} onto AD-char was higher than the capacity of commercial active carbon (103 μmol g^{-1}) or biochar derived from hardwood (106 μmol g^{-1}) (Chen *et al*. 2011; Ulmanu *et al*. 2003). Although the adsorption capacity was still lower than other sorbents such as synthetic polymers (Wang *et al*. 2010), the AD-char had the advantage of being produced from municipal organic waste, leading to the low cost of raw material and providing additional value during waste treatment *via* anaerobic digestion. This result demonstrates that biochar production from AD residue could provide an efficient metal adsorbent.

Metal ion adsorptions onto these two biochars were fitted using the Freundlich and Langmuir isotherms (Table 5). The Langmuir isotherm had better fitting performance for the predominant Cu^{2+} adsorption (R^2=0.93-0.98). The Langmuir isotherm is valid for monolayer sorption onto a surface with a finite number of identical sites, so Cu^{2+} adsorption onto biochars may primarily be monolayer sorption. The saturation adsorption of Cu^{2+} onto AD-char calculated by the Langmuir isotherm was 206.17 μmol g^{-1}, which was higher than the calculated value (173.99 μmol g^{-1}) of E-char. The adsorption parameter *b* was higher for AD-char than it was for E-char, which suggests that AD-char was more favorable for metal adsorption (Kalavathy *et al*. 2005).

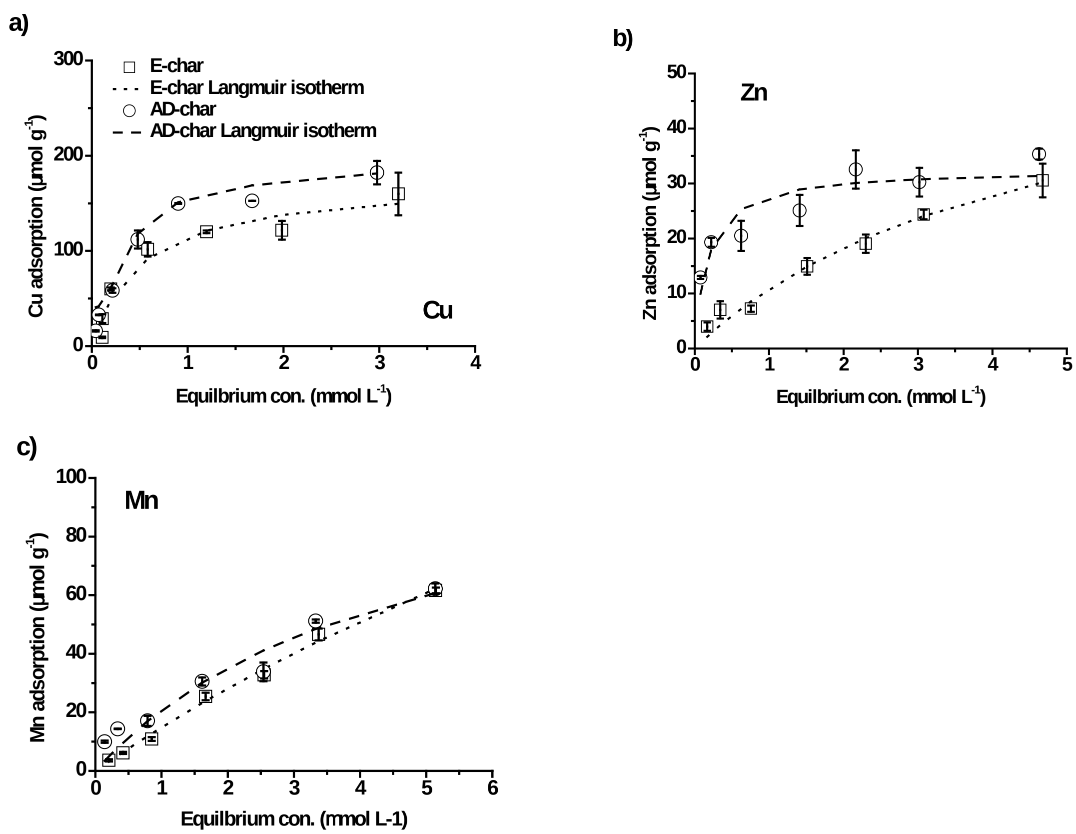

Fig. 4. Adsorption isotherm of metals on biochars

Table 3. Comparison of the Radius [a] and Hydrolysis constant [b] of Different Metals at 25 °C

	Crystal radius (Å)	Stokes` law radius (Å)	Hydrated radius (Å)	Hydrolysis constant pK [c]
Cu^{2+}	0.72	3.25	4.19	7.7
Zn^{2+}	0.74	3.49	4.30	9.0
Mn^{2+}	0.80	3.68	4.38	10.7

[a] The data of metal ionic radius was obtained from Nightingale 1959.
[b] The values of pK were obtained from Atanassova 1999 and Yavuz *et al.* 2003.
[c] $pK = - Log (C_{MOH}{}^{+} \cdot C_{H}{}^{+} / C_{M}{}^{2+})$

Table 4. Comparison of the Cu^{2+} Adsorption Capacity of Biochar

	Metal adsorption capacity	Reference
AD-char	182 μmol g^{-1}	This study
E-char	160 μmol g^{-1}	This study
Cellulose pulp waste	78 μmol g^{-1}	Ulmanu *et al*. 2003
Food waste	44 μmol g^{-1}	Zheng *et al.* 2008
Commercial active carbon	103 μmol g^{-1}	Ulmanu *et al*. 2003
Hardwood-biochar	106 μmol g^{-1}	Chen *et al*. 2011
synthetic PS-EDTA resin	658 μmol g^{-1}	Wang *et al.* 010

Table 5. Fitted Isotherms for Metal Adsorption by Biochars

	Cu		Zn		Mn	
	E-char	AD-char	E-char	AD-char	E-char	AD-char
Freundlich isotherm						
K_F (μmol g^{-1})	1.11	2.70	0.17	4.89	0.03	0.72
1/n	0.64	0.56	0.61	0.23	0.91	0.51
R^2	0.76	0.94	0.97	0.95	0.99	0.96
Langmuir isotherm						
Q_0 (μmol g^{-1})	173.99	206.17	59.12	32.58	271.10	113.41
b	$1.92*10^{-3}$	$2.29*10^{-3}$	$2.24*10^{-4}$	$5.61*10^{-3}$	$5.79*10^{-5}$	$2.24*10^{-4}$
R^2	0.93	0.98	0.97	0.78	0.99	0.92

Influence of pH on Metal Adsorption of Biochars

As shown in Figs. 5a to 5c, for both AD-char and E-char, a change in initial pH influenced Cu^{2+}, Zn^{2+}, and Mn^{2+} adsorption. In particular, for E-char, Cu^{2+} and Zn^{2+} adsorptions in the treatment with an initial pH of 6 were 30.3±0.2 µmol g^{-1} and 8.74±0.31 µmol g^{-1}, respectively, which were about twice those with an initial pH of 3, while Mn^{2+} adsorption was 8.47±0.21 µmol g^{-1}, which was 1.3 times that in the treatment with an initial pH of 3. The metal adsorption onto E-char was increased with increased initial solution pH. However, the metal adsorption varied less among the treatments with AD-char. Cu^{2+} adsorption onto AD-char ranged from 32.8 µmol g^{-1} to 36.6 µmol g^{-1}, while Zn^{2+} and Mn^{2+} adsorptions were around 19.3 µmol g^{-1} to 28.0 µmol g^{-1} and 14.4 µmol g^{-1} to 19.1 µmol g^{-1}, respectively. The increase of initial solution pH from 3 to 6 did not significantly increase the metal adsorption onto AD-char, which was different from that by E-char. In addition, with the same initial pH, metal ion adsorption onto AD-char was always significantly higher (P < 0.05) than that onto E-char. For instance, in the treatments with an initial pH of 3, Cu^{2+} adsorption onto AD-char was more than 2.3 times that onto E-char. Again, AD-char showed higher metal adsorption capacity from acidic wastewater. One possible reason was that AD-char had a higher neutralization capacity than E-char, which can lead to higher pH (as shown in Fig. 5d) and prompt metal ion adsorption (Mukherjee *et al*. 2011). According to the pH titration experiment (data not shown), the equilibrium pH of different $NaNO_3$ solutions increased to higher values in treatments with AD-char compared to those with E-char. For example, the strong acidic solution (pH=2.1) was neutralized to pH 6.78 after reaction with AD-char, whereas the pH remained acidic (pH=2.7) with the E-char. Thus, metal ion adsorption from acidic wastewater would increase under higher pH neutralized by AD-char, which results in AD-char having a higher adsorption capacity than E-char.

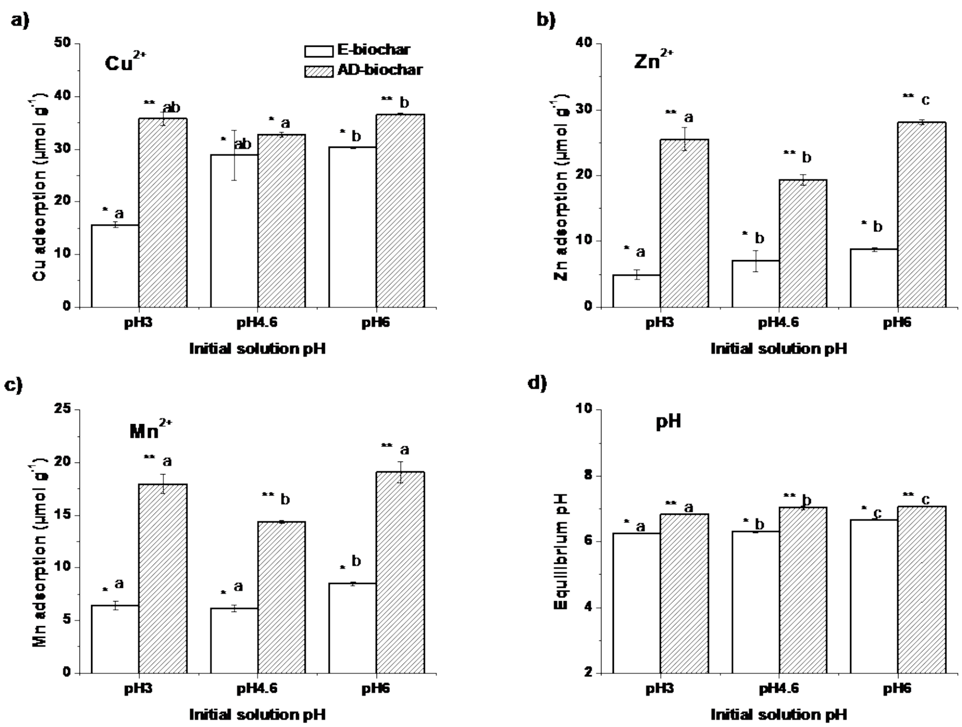

Fig. 5. Metal adsorption and pH change in different initial pH treatment exposed to 10 g L^{-1} biochar. Bars with the same letter were not significantly different at the 0.05 level among the treatments with the same biochar. Bars with * were significantly different from bars with ** in the treatment with same initial pH at the 0.05 level.

Modeling with a Surface Complexation Model

Modeling of the surface functional sites on biochars

As simulated by the surface complexation model using the pH titration experimental results, the distributions of surface functional sites (XOH_2^+, XOH, and XO^-) on biochars are shown in Fig. 6. The total surface functional sites of biochars needed for simulation used data from the Boehm titration. As optimized by the SFM, the pK^{int}_{a1} and pK^{int}_{a2} for AD-char were 5.75 and -10.20, respectively, and were 2.15 and -10.70 for E-char, respectively. When the pH exceeded 7.9, the density of negative surface sites (XO^-) on AD-char was higher than the density of positive surface sites (XOH_2^+), in which the net surface charge became negative. In contrast, for the E-char, when the pH exceeded 6.5, the net surface charge became negative. However, the increasing rate of negative surface charge on E-char with increased pH was slower than that on AD-char, which resulted in a lower fraction of surface sites present as negative charges on E-char, compared to AD-char, at the same pH. For instance, when the pH increased to 10, the net surface charge of E-char was less than 0.5 mmol g^{-1}, whereas the value was 1.3 mmol g^{-1} for AD-char. One possible reason for this condition is that AD-char had more surface functional groups, particularly alkaline groups, as shown in Table 1. Thus, at high pH, the surface deprotonation reactions of those groups would lead to more negative XO^- present on AD-char, which increases the potential of surface complexation between AD-char and the H^+ ion or metal ions.

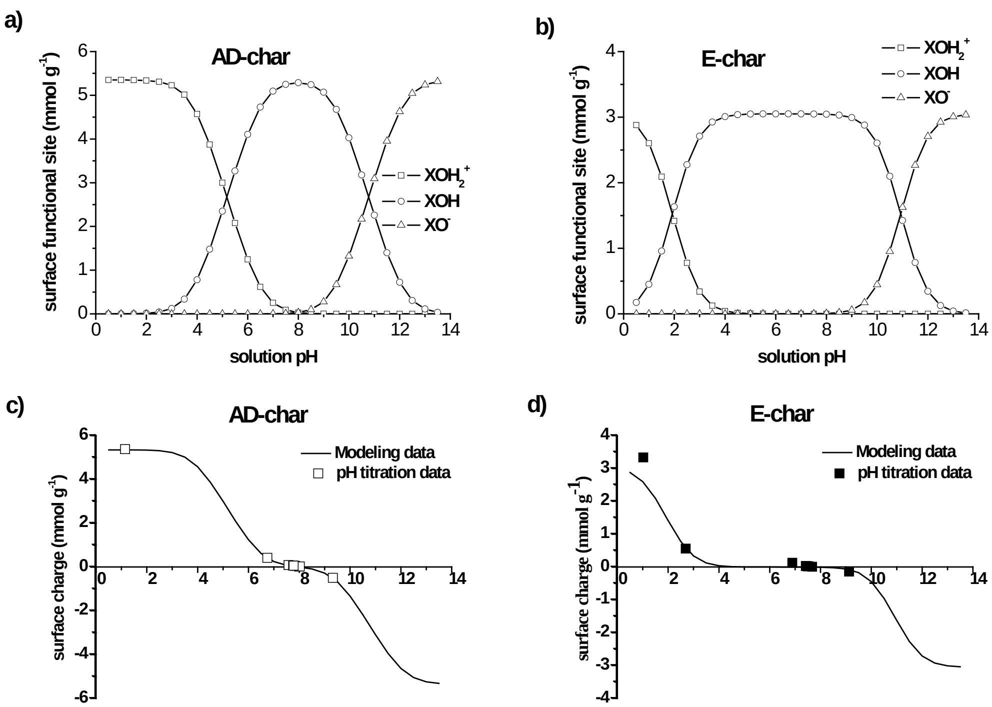

Fig. 6. Distributions of surface functional sites and surface charges on biochars as functions of pH simulated by the SCM

Modeling of copper ion adsorption on biochars with a surface complexation model

As discussed above, Cu^{2+} adsorption was predominant among the three metal ions. Thus, the surface complexation model was further used to simulate Cu^{2+} adsorption using the adsorption experimental data, which could increase understanding of the adsorption mechanism. As optimized by FITEQL 4.0, the complexation constant pk_{Cu} was -4.70 for AD-char and -4.68 for E-char. As shown in Fig. 7, the fraction of $XOCu^+$ adsorbed onto biochars increased with increasing pH of less than 8.6, and then gradually released from the biochar surface and turned into $Cu(OH)_2$ after adsorption reached the maximum. At the increased stage, the fraction of $XOCu^+$ reached 50% at pH 6.25 for AD-char, which was close to the endpoint of pH 6.2 for E-char. However, at the decreased stage, the fraction of $XOCu^+$ on AD-char remained 50% at pH 11.5, while the fraction for E-char was less than 20% at the same pH, at which the point of 50% retention was about pH 11. Thus, AD-char could last for a longer pH range for $XOCu^{+}$ adsorption, which may be explained by its high negative surface charge at high pH. In addition, because AD-char had a higher neutralization capacity, the equilibrium pH after reaction with acidic wastewater would be higher than for E-char, in which the fraction of $XOCu^{+}$ on AD-char would be higher than for E-char and could even reach 100% under certain conditions. Again, AD-char showed higher metal adsorption capacity than E-char, which indicates its great potential for environmental remediation.

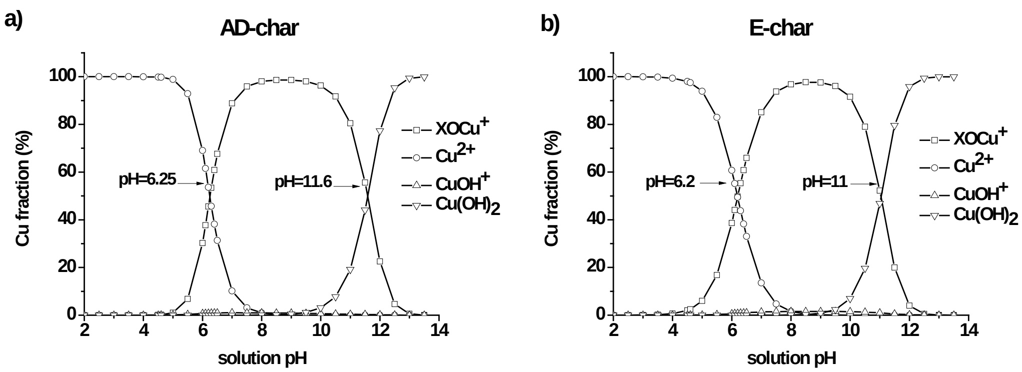

Fig. 7. Simulations of copper ion speciation and distributions of surface sites on biochars as functions of pH with 0.4 mmol L^{-1} copper solution exposed to 10 g L^{-1} biochar

CONCLUSIONS

1. Biochar derived from the AD residues of garden waste showed a high capacity for metal adsorption, suggesting that biochar production using AD residue of MSW could generate efficient metal adsorbents for the remediation of metal-contaminated wastewater.
2. The kinetic adsorption characteristics were well described by the pseudo second-order model, which indicates that the chemisorption mechanism controls the metal adsorption onto AD-char.
3. The adsorption isotherm of metal adsorption onto AD-char was better fitted by the Langmuir isotherm, which suggests monolayer adsorption.
4. As simulated by the surface complexation model, the metal adsorption capacities of AD-char increased with increasing pH, which suggests that the presence of surface alkaline functional groups may contribute to the metal adsorption capacity of biochars.

ACKNOWLEDGMENTS

This work was financially supported by grants from the Natural Science Foundation of China (41301328), the National High-Tech R & D Program of China (863 Program, 2012AA06A204-2), and the Fujian Science Foundation (2012Y0067).

REFERENCES CITED

Al-Hamdan, A. Z., and Reddy, K. R. (2005). "Surface speciation modeling of heavy metals in kaolin: Implications for electrokinetic soil remediation processes," *Adsorption* 11(5-6), 529-546.

Arvanitoyannis, I.S., and Varzakas, T.H. (2008). "Vegetable waste treatment: comparison and critical presentation of methodologies," *Crit. Rev. Food Sci.* 48, 3, 205-247.

Atanassova, I. (1999). "Competitive effect of copper, zinc, cadmium and nickel on ion adsorption and desorption by soil clays," *Water Air Soil Pollut* 113(1-4), 115-125.

Beesley, L., Moreno-Jiménez, E., Gomez-Eyles, J. L., Harris, E., Robinson, B., and Sizmur, T. (2011). "A review of biochars's potential role in the remediation, revegetation and restoration of contaminated soils," *Environ. Pollut.* 159(12), 3269-3282.

Cao, X. D., Ma, L. N., Gao, B., and Harris, W. (2009). "Dairy-manure derived biochar effectively sorbs lead and atrazine," *Environ. Sci. Technol.* 43(9), 3285-3291.

Cao, X., and Harris, W. (2010). "Properties of dairy-manure-derived biochar pertinent to its potential use in remediation," *Bioresource Technol.* 101(14), 5222-5228.

Chen, X. C., Chen, G. C., Chen, L. G., Chen, Y. X., Lehmann, J., McBride, M. B., and Hay, A. G. (2011). "Adsorption of copper and zinc by biochars produced from pyrolysis of hardwood and corn straw in aqueous solution," *Bioresource Technol.* 102, 8877-8884.

Dong, X. L., Ma, L. N., and Li, Y. C. (2011). "Characteristics and mechanisms of hexavalent chromium removal by biochar from sugar beet tailing," *J. Hazard. Mater.* 190(1-3), 909-915.

Guo, X. Y., Zhang, S. Z., and Shan, X. Q. (2008). "Adsorption of metal ions on lignin," *J. Hazard. Material.* 151(1), 134-142.

Gupta, V. K., Ali, I., Saleh, T. A., Siddiqiu, M. N., and Agarwal, S. (2012). "Chromium removal from water by activated carbon developed from waste rubber tires," *Environ. Sci. Pollut. Res.* 20(3), 1261-1268.

Hanay, O., Hasar, H., Kocer, N. N., and Aslan, S. (2008). "Evaluation for agricultural usage with speciation of heavy metals in a municipal sewage sludge," *B. Environ. Contam. Tox.* 81(1), 42-46.

Herbelin, A. L., and Westall, J. C. (1999). *FITEQL: A computer program for determination of chemical equilibrium constants from experimental data, version 4.0.* Department of Chemistry, Oregon State University.

Ho, Y. S. (2006). "Second-order kinetic model for the sorption of cadmium onto tree fern: A comparison of linear and non-linear methods," *Water Research* 40(1), 119-125.

Inyang, M., Gao, B., Pullammanappallil, P., Ding, W. C., and Zimmerman, A. R. (2010). "Biochar from anaerobically digested sugarcane bagasses," *Bioresource Technol.* 101(22), 8868-8872.

Inyang, M., Gao, B., Yao, Y., Xue, Y. W., Zimmerman, A. R., Pullammanappallil, P., and Cao, X. D. (2012). "Removal of heavy metals from aqueous solution by biochars derived from anaerobically digested biomass," *Bioresource Technol.* 110, 50-56.

Jiang, T. Y., Jiang, J., Xu, R. K., and Li, Z. (2012). "Adsorption of Pb(Ⅱ) on variable charge soils amended with rice-straw derived biochar," *Chemosphere* 89(3), 249-256.

Kalavathy, M. H., Karthikeyan, T., and Rajgopal, S. (2005). “Kinetic and isotherm studies of Cu(II) adsorption onto H_3PO_4-activated rubber wood sawdust,” *J. Colloid Interf. Sci.* 292(2), 354-362.

Lehmann, J., Rillig, M. C., Thies, J., Masiello, C. A., Hockaday, W. C., and Crowley, D. (2011). “Biochar effects on soil biota – A review,” *Soil Biol. Biochem.* 43(9), 1812-1836.

Melo, L .C. A., Coscione, A. R., Abreu, C. A., Puga, A. P., and Camargo, O. A. (2013). “Influence of pyrolysis temperature on cadmium and zinc sorption capacity of sugar cane straw-derived biochar,” *BioRes.* 8(4), 4992-5004.

Mohan, D., Sharma, R., Singh, V. K., Steele, P., and Pittman Jr., C. U. (2012). “Fluoride removal from water using bio-char, a green waste, low-cost adsorbent: Equilibrium uptake and sorption dynamics modeling,” *Ind. Eng. Chem. Res.* 51(2), 900-914.

Mukome, F. N. D., Zhang, X. M., Silva, L. C. R., Six, J., and Parikh, S. J. (2013). “Use of chemical and physical characteristics to investigate trends in biochar feedstocks,” *J. Agric. Food Chem.* 61(9), 2196-2204.

Mukherjee, A., Zimmerman, A. R., and Harris, W. (2011). “Surface chemistry variations among a series of laboratory-produced biochars,” *Geoderma* 163(3), 247-255.

Nightingale, Jr E. R. (1959). “Phenomenological theory of ion solvation. Effective radii of hydrated ions,” *J. Phys. Chem.* 63(9), 1381-1387.

Qiu, Y. P., Cheng, H. Y., Xu, C., and Sheng, G. D. (2008). “Surface characteristics of crop-residue-derived black carbon and lead(II) adsorption,” *Water Research* 42(3), 567-574.

Rangel-Mendez, J. R., and Streat, M. (2002). “Adsorption of cadmium by activated carbon cloth: Influence of surface oxidation and solution pH,” *Water Research* 36(5), 1244-1252.

Rapport, J. L., Zhang, R. H., Williams, R. B., and Jenkins, B. M. (2012). “Anaerobic digestion technologies for the treatment of municipal solid waste,” *Int. J. Environment and Waste management* 9(1), 100-122.

Robertson, A. P., and Leckie, J. O. (1997). “Cation binding predictions of surface complexation models: Effects of pH, ionic strength, cation loading, surface complex, and model fit,” *J. Colloid Interf. Sci.* 188(2), 444-472.

Sud, D., Mahajan, G., and Kaur, M. P. (2008). “Agricultural waste material as potential adsorbent for sequestering heavy metal ions from aqueous solutions – A review,” *Bioresource Technol.* 99(14), 6017-6027.

Sun, L., Wan, S. G., and Luo, W. S. (2013). “Biochars prepared from anaerobic digestion residue, palm bark, and eucalyptus for adsorption of cationic methylene blue dye: Characterization, equilibrium, and kinetic studies,” *Bioresource Technol.* 140, 406-413.

Ulmanu, M., Maran, E., Fernandez, Y. Castrillon, L., Anger, I., and Dumitriu, D. (2003). “Removal of copper and cadmium ions from diluted aqueous solutions by low cost and waste material adsorbents,” *Water Air Soil Pollut.* 142(1-4), 357-373.

Uchimiya, M., Lima, I. M., Klasson, K. T., and Wartelle, L. H. (2010). “Contaminant immobilization and nutrient release by biochar soil amendment: Roles of natural organic matter,” *Chemosphere* 80(8), 935-940.

Wang, L. Y., Yang, L. Q., Li, Y. F., Zhang, Y., Ma, X. J., and Ye, Z. F. (2010). “Study on adsorption mechanism of Pb(II) and Cu(II) in aqueous solution using PS-EDTA resin,” *Chem. Eng. J.* 163(3), 364-372.

Xu, N.Z., Yuan, X.Y., and Tao, Y.X. (2003). "Influence of the mining of sulfur-polymetallic deposits on the water environment – a case study of the mineral exploitation in the Datian area, Fujian". *Geol. Bull. China* 22,718-724.

Xu, X. Y., Cao, X. D., Zhao, L., Wang, H. L., Yu, H. R., and Gao, B. (2012). "Removal of Cu, Zn, and Cd from aqueous solutions by the dairy manure-derived biochar," *Environ. Sci. Pollut. R.* 20(1), 358-368.

Xue, Y. W., Gao, B., Yao Y., Inyang, M., Zhang, M., Zimmerman, A. R., Ro, K. S. (2012). "Hydrogen peroxide modification enhances the ability of biochar (hydrochar) produced from hydrothermal carbonization of peanut hull to remove aqueous heavy metals: batch and column tests," *Chem. Eng. J.* 200-202, 673-680.

Yao, Y., Gao, B., Inyang, M., Zimmerman, A. R., Cao, X. D., Pullammanappallil, P., and Yang, L. Y. (2011). "Biochar derived from anaerobically digested sugar beet tailings: Characterization and phosphate removal potential," *Bioresource Technol.* 102, 6273-6278.

Yavuz, Ö., Altunkaynak, Y., Güzel, F. (2003). "Removal of copper, nickel, cobalt and manganese from aqueous solution by kaolinite," *Water research* 37(4), 948-952.

Yuan, X. Z., Shi, X. S., Zeng, S. J., and Wei, Y. L. (2011). "Activated carbons prepared from biogas residue: Characterization and methylene blue adsorption," *J. Chem. Technol. Biotechnol.* 86(3), 361-366.

Zhang, R. H., El-Mashad, H. M., Hartman, K., Wang, F. Y., Liu, G. Q., Choate, C., and Gamble, P. (2007). "Characterization of food waste as feedstock for anaerobic digestion," *Bioresource Technol.* 98(4), 929-935.

Zhao, L., Cao, X. D., Mašek, O., and Zimmerman, A. (2013). "Heterogeneity of biochar properties as a function of feedstock sources and production temperatures," *J. Hazard. Mater.* 256-257, 1-9.

Zheng, W., Li, X. M., Wang, F., Yang, Q., Deng, P., and Zeng, G. M. (2008). "Adsorption removal of cadmium and copper from aqueous solution by areca – A food waste," *J. Hazard. Material.* 157(2), 490-495.

Article submitted: October 31, 2013; Peer review completed: December 22, 2013; Revised version accepted: March 11, 2014; Published: March 19, 2014.